www.sciencemag.org/content/363/6426/538/suppl/DC1

Supplementary Materials for

Intense threat switches dorsal raphe serotonin neurons to a paradoxical operational mode

Changwoo Seo, Akash Guru, Michelle Jin, Brendan Ito, Brianna J. Sleezer, Yi-Yun Ho, Elias Wang, Christina Boada, Nicholas A. Krupa, Durgaprasad S. Kullakanda, Cynthia X. Shen, Melissa R. Warden*

*Corresponding author. Email: mrwarden@cornell.edu

Published 1 February 2019, *Science* **363**, 538 (2019)
DOI: 10.1126/science.aau8722

This PDF file includes:

Materials and Methods

All procedures conformed to guidelines established by the National Institutes of Health and have been approved by the Cornell University Institutional Animal Care and Use Committee.

Subjects

SERT-Cre (Ross McDevitt, NIH/NIDA & Xiaoxi Zhuang, University of Chicago) and Vgat-Cre (The Jackson Laboratory, Bar Harbor, ME) mice (postnatal 3-6 months) were used for 5-HT- and GABA-specific viral vector expression. All Cre driver lines were fully backcrossed to C57BL/6J mice. All mice were male and housed in groups, and were maintained on a 12-hour reverse light-dark cycle with *ad libitum* access to food and water, except during approach conditioning.

Viral vectors

For photometry and microendoscopy experiments, we used AAV5-CAG-FLEX-GCaMP6s (Penn Vector Core, Philadelphia, PA), AAVdj-Ef1α-DIO-GCaMP6m (Stanford Vector Core, Stanford, CA), or AAV5-CAG-FLEX-GFP (UNC Vector Core, Chapel Hill, NC). For optogenetic experiments, we used AAV5-Ef1α-DIO-hChR2(H134R)-eYFP or AAV5-Ef1α-DIO-eYFP (UNC Vector Core, Chapel Hill, NC).

Surgery

Mice were deeply anesthetized with isoflurane (5%). Fur was trimmed, and mice were placed in a stereotaxic frame (Kopf Instruments, Tujunga, CA). A heating pad was used to prevent hypothermia. Isoflurane was delivered at 1-3% throughout surgery; this level was adjusted to maintain a constant surgical plane. Ophthalmic ointment was used to protect the eyes. Buprenorphine (0.05 mg/kg, subcutaneous) was given before the start of surgery. A mixture of 0.5% lidocaine and 0.25% bupivacaine (100 μL) was injected subdermally along the incision line. The scalp was disinfected with betadine and alcohol. A midline incision exposed the skull, which was thoroughly cleaned, and a craniotomy was made above the DRN. Virus was targeted to the DRN (-4.5 AP, 0.0 ML, -3.3 & -3.0 DV), and slowly pressure injected (100 nl/min) using a 10 μL Hamilton syringe (nanofil; WPI, Sarasota, FL), a 33 gauge beveled needle, and a micro-syringe pump controller (Micro 4; WPI, Sarasota, FL). After each injection the needle was left in place for 10 minutes and then slowly withdrawn.

For photometry and microendoscopy experiments, a total of 700 nl (350 nl at each DV site) of vector was injected. For optogenetic experiments, a total of 800 nl (400 nl at each DV site) of vector was used. For photometry and optogenetic experiments an optical fiber embedded in a metal ferrule was implanted at 15° (-4.5 AP, 0.5 ML, -2.8 DV). A 400 μm diameter, 0.48 NA optical fiber (Doric Lenses, Québec, Canada) was used for photometry experiments, and a 200 μm diameter, 0.22 NA optical fiber (Thorlabs Inc., Newton, NJ) was used for optogenetic experiments. For microendoscopy experiments, animals were implanted with a 6 mm long, 500 μm diameter GRIN lens (Inscopix, Palo Alto, CA) at 15° (-4.5 AP, 1.1 ML, -3.3 DV). A layer of metabond (Parkell, Inc., Edgewood, NY) and dental acrylic (Lang Dental Manufacturing, Wheeling, IL) was applied to firmly hold the implant in place, and the surrounding skin was sutured closed. Post-operative buprenorphine (0.05 mg/kg), carprofen (5 mg/kg), and lactated ringers (500 μL) were administered subcutaneously. For microendoscopy, a baseplate was implanted above the GRIN lens after 3 weeks. Virus was allowed to express for a minimum of 3 weeks before behavioral testing.

Fiber photometry

Fiber photometry was performed as previously described. 473 nm and 405 nm data were collected for all GCaMP and GFP photometry experiments. 473 nm and 405 nm diode lasers (Omicron Luxx, Rodgau-Dudenhofen, Germany) were modulated at 700 Hz and 500 Hz, respectively, using a dual optical chopper (New Focus Model 3502, Newport, Irvine, CA). Both laser beams were combined using a mirror (KM100-E02, Thorlabs, Newton, NJ) and a dichroic filter (LM01-427, Semrock, Rochester, NY), and the power was adjusted using a neutral density filter to 15-100 μW. Power-adjusted laser beans were aligned to a fluorescence filter cube (DFMB, Thorlabs, Newton, NJ), where the excitation beams were reflected with a dichroic filter (FF495, Semrock, Rochester, NY), collimated (F240FC-A with AD11F, Thorlabs, Newton, NJ), and coupled to an optical patch cord (400 μm, Doric Lenses, Quebec, Canada). Emitted fluorescence was passed through a dichroic filter (FF495, Semrock, Rochester, NY) and a bandpass filter (FF03-525/50, Semrock, Rochester, NY), and was collected by a femtowatt photoreceiver (New Focus 2151, Newport, Irvine, CA). Outputs from the photoreceiver were directed through two lock-in amplifiers (SR810 DSP, Stanford Research System, Sunnyvale, CA), digitized using a DAQ (U6 pro, LabJack, Lakewood, CL) at a sampling rate of 250 Hz, and recorded by custom-modified LabJack software.

Optogenetic stimulation

During behavioral testing an external optical fiber (200 μm diameter, 0.22 NA, Doric Lenses, Québec, Canada) was coupled to the implanted fiber optic with a zirconia sleeve. An optical commutator allowed for unrestricted rotation (Doric Lenses, Québec, Canada). Optical stimulation was provided with a 100 mW 473 nm diode pumped solid state laser (OEM Laser Systems, Inc., Salt Lake City, UT) and controlled by a Master-8 stimulus generator (A.M.P.I., Jerusalem, Israel). Trains of 25 Hz, 10 ms light pulses were used for all ChR2 experiments. Stimulation experiments used 6 mW light (47.73 mW/mm^2 at the fiber tip), with stimulation epoch length dependent on the behavioral task.

Microendoscopy

Prior to behavioral testing animals were briefly anaesthetized to attach the microendoscope to the baseplate (Inscopix, Palo Alto, CA). Imaging data was acquired at 20 Hz for 15 minutes in the OFT and 15 minutes in the TST. Fluorescence videos were preprocessed, down-sampled to 10 Hz, spatially filtered, and motion corrected using Inscopix software. Videos were exported and processed with MIN1PIPE (*29*), where background was subtracted, motion was corrected, and neural signal was extracted. MIN1PIPE seeds were picked manually, and code was modified to remove the > 0 constraint on temporal components. Data was processed separately for the OFT and the TST.

Behavioral testing: open field test (OFT), tail suspension test (TST), and wheel

Mouse behavior was recorded at 30 fps with a USB 3.0 camera (Chameleon3, Pointgrey, Richmond, BC, Canada) during all behavioral testing sessions. A Labjack DAQ (U6 pro, LabJack, Lakewood, CL) was used to acquire all behavioral data. The sequence of behavioral tests follows the individual test descriptions.

OFT (photometry): A 50 x 50 cm arena made of white Plexiglas was divided into large (50 x 42 x 37.5 x 32 cm, used for open field testing) and small (used for wheel testing) subsections. Testing took place under bright room light. Mice were placed in the center of the large arena at the start of each OFT and allowed to freely explore for 6 minutes. Movement was tracked using Ethovision (Noldus, Leesburg, VA).

Wheel (photometry): 4-6 weeks after surgery, a running wheel (Ware Manufacturing, Amazon) was introduced to the home cage for about a week for acclimation. During testing, the running wheel was placed into the small subsection of the OFT, described above. Animals were placed into this section and allowed to freely engage in running behavior on the wheel for 20 minutes. Wheel movement was captured by an optical encoder (E4T 200 cycles per revolution, US Digital, Vancouver, WA) attached to the bottom part of the wheel shaft.

TST (photometry): The mouse's tail was taped to a 40 cm high horizontal bar, and the mouse was suspended by its tail for 6 minutes. Struggling behavior was recorded using an accelerometer taped to the tail.

Testing sequence (photometry): On photometry recording days, mice were plugged into an optical patch cord connected to the fiber photometry data acquisition rig and were exposed to the following series of behavioral experiments: OFT – Wheel – OFT – TST – OFT. Mice were moved by the experimenter between each behavioral test without disconnection from the fiber photometry system so that data could be continuously recorded. Conditions and timing for each test were as described above. While the animal was in the second OFT, wheel running data were analyzed. If mice performed multiple bouts of wheel running with a duration greater than five seconds on the wheel, mice were moved from the OFT to the TST, and then back to the last OFT. If running behavior did not meet this criteria, mice were brought back to the home cage and tested on subsequent days; if criteria were never met, mice were excluded from further study.

OFT (optogenetics): A 50 × 50 cm arena made of white Plexiglas was used as an open field under bright room light. Mice were placed in the center of the arena at the start of each session. The stimulation protocol used for this open-field test replicated the phasic optogenetic stimulation protocol outlined by Correia et al. (2017). The protocol consisted of 5-minute blocks alternating between stimulation and no-stimulation. During stimulation blocks, light was delivered for 3 seconds followed by a 7-second pause, a pattern that repeated throughout the block. The session began with a no-stimulation block for a total session time of 30 minutes (OFF-ON-OFF-ON-OFF-ON).

Wheel (optogenetics): A running wheel was introduced to the home cage for acclimation. About a week later, mice were acclimated to the running wheel in the OFT arena, surrounded by temporary walls to provide an enclosed space. On a control day, mice were tethered to a patch cord and allowed to freely run on the wheel for 20 minutes. On a following experimental day, the session began with a 5-minute no-stimulation block followed by 3-minute blocks alternating between stimulation and no-stimulation for a total session time of 20 minutes (OFF-ON-OFF-ON-OFF-ON). For Vgat::ChR2 groups, 25 Hz 10 ms light pulses were continuously delivered during the stimulation block.

TST (optogenetics): Mice were tethered to a patch cord and the tail was taped to an accelerometer attached to a horizontal bar 40 cm from the ground. The protocol consisted of 3-minute blocks alternating between stimulation and no-stimulation blocks. The session began with a no-stimulation block for a total session time of 18 minutes (OFF-ON-OFF-ON-OFF-ON). For SERT::ChR2 groups, 25 Hz 10 ms light pulses were delivered for 3 seconds followed by a 7-second pause, a pattern that repeated throughout the block. For Vgat::ChR2 groups, 25 Hz 10 ms light pulses were continuously delivered during the stimulation block.

Behavioral testing: reward approach and shock avoidance tasks

Reward approach and shock avoidance tasks were performed in metal rectangular shuttle boxes divided into two equal compartments by Plexiglas semi-partitions, which allowed animals to move freely between compartments. A 17.25” W x 6.75” D x 10” H shuttle box (MedAssociates, Fairfax, VT) was used for SERT::GCaMP, SERT::ChR2, and Vgat::ChR2 experiments, and a 14” W x 7” D x 12” H shuttle box (Coulbourn Instruments, Whitehall, PA) was used for Vgat::GCaMP experiments. All shuttle box experiments were done in the dark. Mice were tracked using infrared detectors located alongside the chambers and an infrared USB 3.0 camera (Chameleon3, Pointgrey, Richmond, BC, Canada). All signals from the shuttle boxes were converted to TTL (SuperPort 16 Output Module, MedAssociates, Fairfax, VT or Habitest Linc Output Converter, Coulbourn Instruments, Whitehall, PA) and collected by the Labjack DAQ (U6 pro, LabJack, Lakewood, CL). For approach experiments, walls at the end of each compartment were equipped with lick spouts for water delivery and lick detection.

Approach conditioning: Mice were water restricted prior to approach conditioning. Body mass was measured daily to maintain at least 80% baseline body weight. For training, a tone (4 kHz or 12 kHz at

60 dB, counterbalanced between approach and avoidance tasks) was played indefinitely until mice crossed the chamber. When crossed, 20 μl of water was delivered to the lick spout in the goal chamber. Tones occurred pseudo-randomly with an average inter-trial interval (ITI) of 40 seconds after water consumption, and mice were given the opportunity to perform 30-50 trials per day. After several days of training, mice were switched to a testing protocol, which used a tone with a maximum 8-second duration. Mice were required to cross the chamber within this 8-second window for successful water delivery. If mice crossed the chamber within 8 seconds, the tone was terminated and water was delivered to the goal compartment. However, if mice did not cross the chamber within 8 seconds, the tone was terminated at 8 seconds and no water was delivered.

Approach (optogenetics): After learning criteria were met, on the control day mice were tethered to a patch cord and performed the behavioral task with no light delivery. On a following experimental day, stimulation light was delivered on every trial, starting at tone onset. Light was always delivered for 3 seconds, regardless of behavioral outcome.

Avoidance conditioning: A tone (4 kHz or 12 kHz, 60 dB, counterbalanced between approach and avoidance tasks) was played for 8 seconds pseudo-randomly with an average ITI of 40 seconds. If mice did not cross the chamber within 8 seconds, electric footshock (0.2 mA - 0.4 mA) was delivered through the grid floor until mice crossed the chamber (escape, or failed avoidance trials). If mice crossed within 8 seconds, the tone terminated and there was no shock (avoidance trials). Animals performed 30-40 trials per day.

Avoidance (optogenetics): After learning criteria were met, on the control day mice were tethered to a patch cord and performed the behavioral task with no light delivery. On a following experimental day, stimulation light was delivered on every trial, starting at tone onset. Light was always delivered for 3 seconds, regardless of behavioral outcome.

Perfusion and histological verification

Following experiments, animals were deeply anesthetized with Fatal-Plus at a dose of 90 mg/kg and transcardially perfused with 20 ml of PBS (phosphate-buffered saline), followed by 20 ml of 4% paraformaldehyde solution. Brains were extracted and stored overnight at 4°C in 4% paraformaldehyde

solution. After 24 hours, brains were transferred to 30% sucrose solution and allowed to equilibrate for at least 3 days. Brains were sectioned coronally (40 μm) on a freezing microtome. Sections were washed in PBS and mounted on slides with PVA-DABCO. Images were acquired using a Zeiss LSM 800 confocal scanning laser microscope with a 20X air objective.

Data analysis

All data analysis and statistical tests were performed using custom-written scripts in MATLAB (MathWorks, Natick, MA) and GraphPad Prism (GraphPad Software, San Diego, CA).

Statistics: Tabulated statistical results are presented in Table S1. Error bars and shaded areas report standard error of the mean (s.e.m.). All statistical tests were two-tailed. Within-subject analyses were performed using the Wilcoxon signed-rank test, and between-subject analyses were performed using the Wilcoxon rank-sum test. All latency comparisons were performed using the Mantel-Cox log-rank test to account for the fact that failed trials in the approach task had unknown true latencies (since, by definition, latencies in these trials were greater than the 8-second cut-off time). This test was developed for population survival analyses, and is appropriate and unbiased for right-censored data of this form. Cross-covariogram confidence intervals were computed using a circular block bootstrap with random block length (*30*).

Fiber photometry: Raw 473 nm and 405 nm channels were low-pass filtered at 20 Hz. The 405 nm reference channel was fit to the 473 nm channel using linear least squares. Relative fluorescence changes, reported as ΔF/F, were calculated using the following equation:

$$\frac{\Delta F}{F_0} = \frac{\text{473 nm signal-fitted 405 nm signal}}{\text{mean 473 nm signal}} \times 100$$

Open Field Test: Movement onsets were defined by at least 2 seconds of < 2 cm/s speed followed by at least 2 seconds of > 2 cm/s speed. Group photometry analyses compared mean ΔF/F 1.5 seconds before and after movement onset. Optogenetic analyses compared ChR2 and eYFP mean speed during the 3-second stimulation period.

Approach task: Speed was thresholded at 3 cm/s to find movement onsets and offsets. Movements to cross the chamber were identified as the last movement onset during the tone. Data analysis only included trials with less than 3 seconds between chamber crossing and the first lick. Movement offsets were defined as < 3 cm/s speed following movement of at least 1 second of < 3 cm/s speed. Group photometry analyses compared mean ΔF/F 1.5 seconds before and after movement onset/offset. Optogenetic speed analyses compared ChR2 and eYFP mean speed during the 3-second stimulation period. Optogenetic latency analyses compared ChR2 and eYFP latency distributions using the log-rank test, discussed above. For these, all failed trials (where the mouse did not cross the chamber within 8 seconds) are grouped together and plotted at the 8-second point, since there is no latency information by definition for these trials. The log-rank statistical test (discussed above) accounts for this feature of latency datasets.

Avoidance task: Speed was thresholded at 1 cm/s to find movement onsets. Trials were divided into avoidance and failed avoidance (escape) trials with latencies respectively smaller or greater than the maximum tone duration (8 seconds). For avoidance trials, movements to cross the chamber were identified as the last movement onset during the tone. For failed avoidance data analysis, we used data from the first avoidance session. Shock-induced movement onsets were identified as the first movement onset during the shock. Movement offsets were defined as < 1 cm/s speed following movement of at least 1 second at > 5 cm/s speed. Group photometry data analysis compared mean ΔF/F 1.5 seconds before and after movement onset. For analyzing within-day response changes, the first avoidance day data was divided into 10 bins (1 pre-shock and 9 post-shock bins). Movement onsets that occurred between shocks (starting 5 seconds after shock and ending 8 seconds before shock) were included in the analysis. For each bin, the group photometry data compared the difference of mean ΔF/F 1.5 seconds before and after movement onset was calculated. Optogenetic speed analyses compared ChR2 and eYFP mean speed during the 3-second stimulation period. Optogenetic latency analyses compared ChR2 and eYFP latency distributions using the log-rank test, discussed above. Although we have complete latency information for avoidance trials, since the moment when the shock was escaped was recorded, we analyzed these data with methods identical to those used for the approach task (the log-rank statistical test) to ensure an equally-powered comparison.

Tail Suspension Test (TST): Data following 2 minutes of TST exposure was used for both photometry and optogenetic data analysis. Movement onset/offset calculation: The z-score of the raw accelerometer data was calculated, and data were rectified, thresholded above 0.3-0.6, and binned into 100 ms bins, so that the value of each bin reflected the fraction of samples above threshold. Movement onset was defined as bin transition from zero to non-zero, with a pre-onset requirement of < 0.02 for at least 2 seconds and a post-onset requirement of >0.06 for at least 2 seconds. If onsets were within 0.8 seconds of each other they were combined. Final movement bouts were required to be at least 2 seconds long. Movement offset was defined as bin transition from non-zero to zero. Movement calculation for display only: Raw accelerometer data were rectified and normalized to the maximum value. Data for each movement onset (as defined above) was averaged and smoothed with a 50-sample moving average. Population photometry data compared mean ΔF/F during 1.5 seconds before and after movement onset. For optogenetic SERT groups, the epochs immediately before (-2 seconds to 0 seconds) and after (0 seconds to 3 seconds) light onset were analyzed. The difference in movement between these two epochs was compared between ChR2-eYFP and eYFP groups. For optogenetic Vgat groups, the time spent mobile during light stimulation was compared between ChR2-eYFP and eYFP groups.

Wheel. Data following 2 minutes of wheel exposure were used for both photometry and optogenetic data analysis. Running rate was calculated as the number of raw optical encoder samples per 100 ms bin. Movement onsets were calculated by normalizing running rate to the maximum for each animal, and then extracting all epochs that met the following criteria: at least 2 seconds of < 0.1 movement followed by at least 5 seconds of > 0.1 movement. Speed was determined using sampling rate and wheel diameter, and was low pass filtered at 5 Hz for display purposes only. Population photometry data compared mean ΔF/F 2 seconds before and 5 seconds after movement onset. For optogenetic Vgat groups the time spent mobile during light stimulation was compared between ChR2-eYFP and eYFP groups.

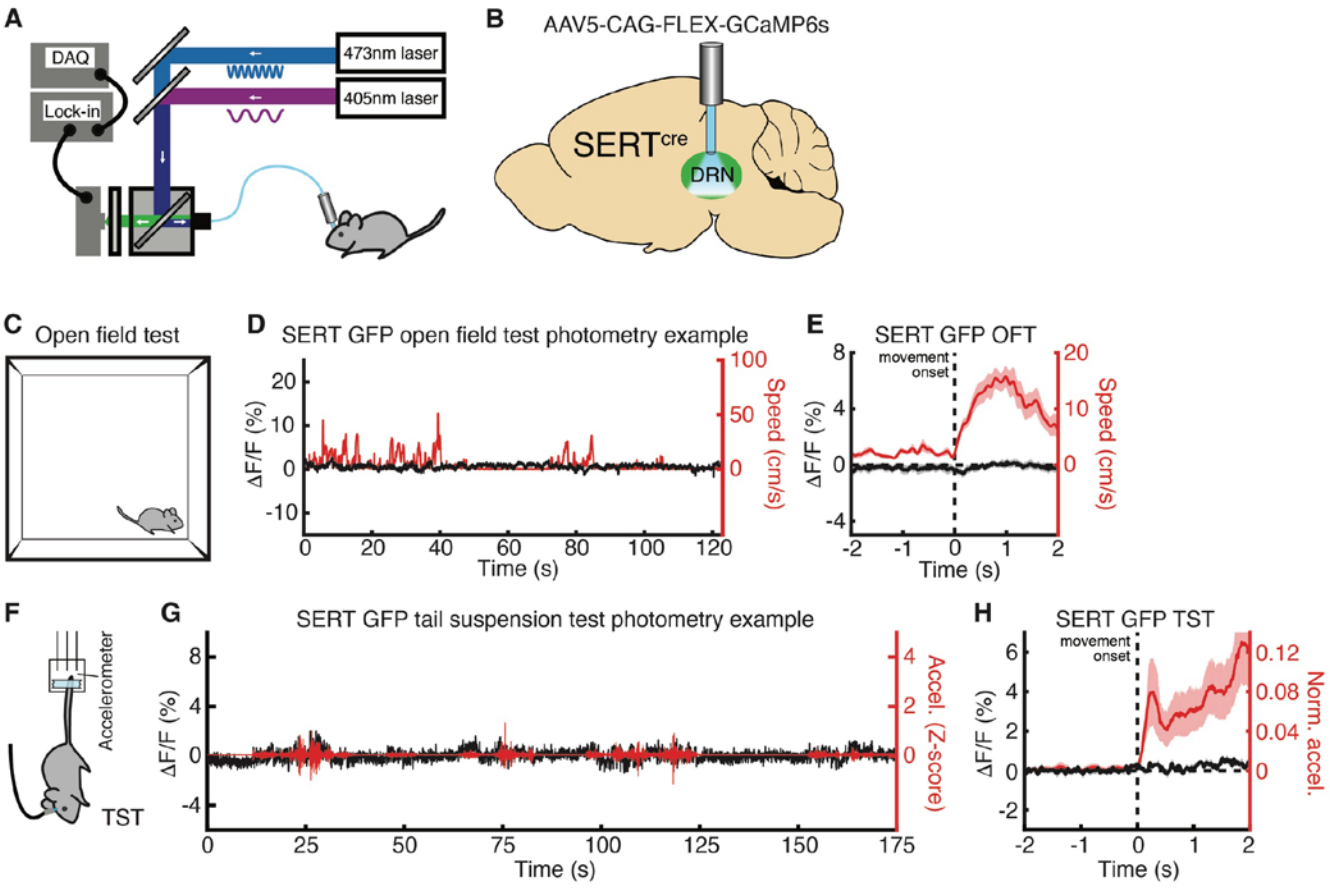

Fig. S1.

(**A**) Fiber photometry schematic. (**B**) Dorsal raphe nucleus (DRN) GCaMP vector and optical fiber placement schematic. (**C**) Open field test (OFT) schematic. (**D**) Example OFT photometry data from a control SERT::GFP mouse. GFP ΔF/F in black, speed in red. (**E**) Mean ΔF/F aligned to OFT movement onset from the same SERT::GFP mouse. (**F**) Tail suspension test (TST) schematic. (**G**) Example TST photometry data from a control SERT::GFP mouse. GFP ΔF/F in black, movement in red. (**H**) Mean ΔF/F aligned to TST movement onset from the same SERT::GFP mouse. X- and Y-axes for all panels match the GCaMP data in the main figures.

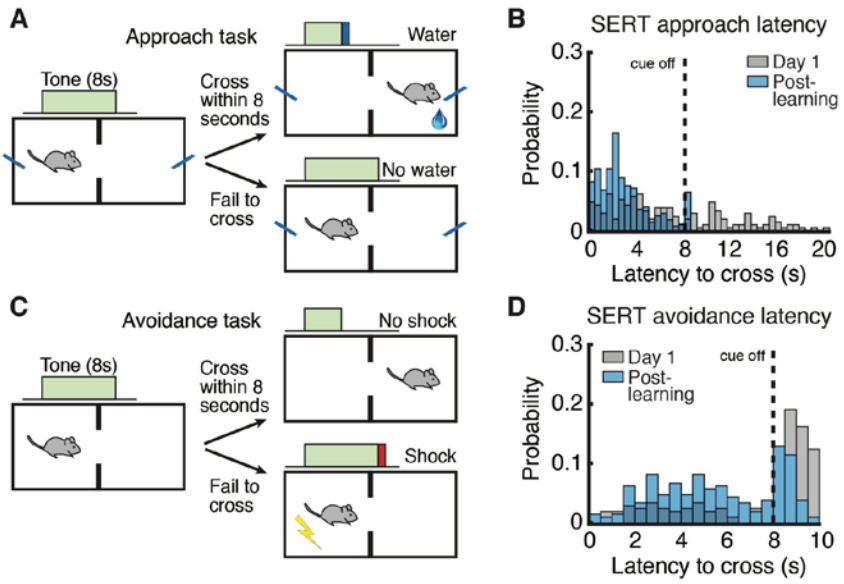

Fig. S2

(**A**) Approach task schematic. (**B**) Latency to cross after cue onset distribution, approach task, day 1 and post-learning (SERT::GCaMP, n=7; $P < 0.0001$, log-rank test). Latency data were not collected for failed approach trials post-learning, but are binned here at 8 s for display only (not for statistical analysis). (**C**) Avoidance task schematic. (**D**) Latency to cross after cue onset distribution, avoidance task, day 1 and post-learning (SERT::GCaMP, n=7; $P < 0.0001$, log-rank test).

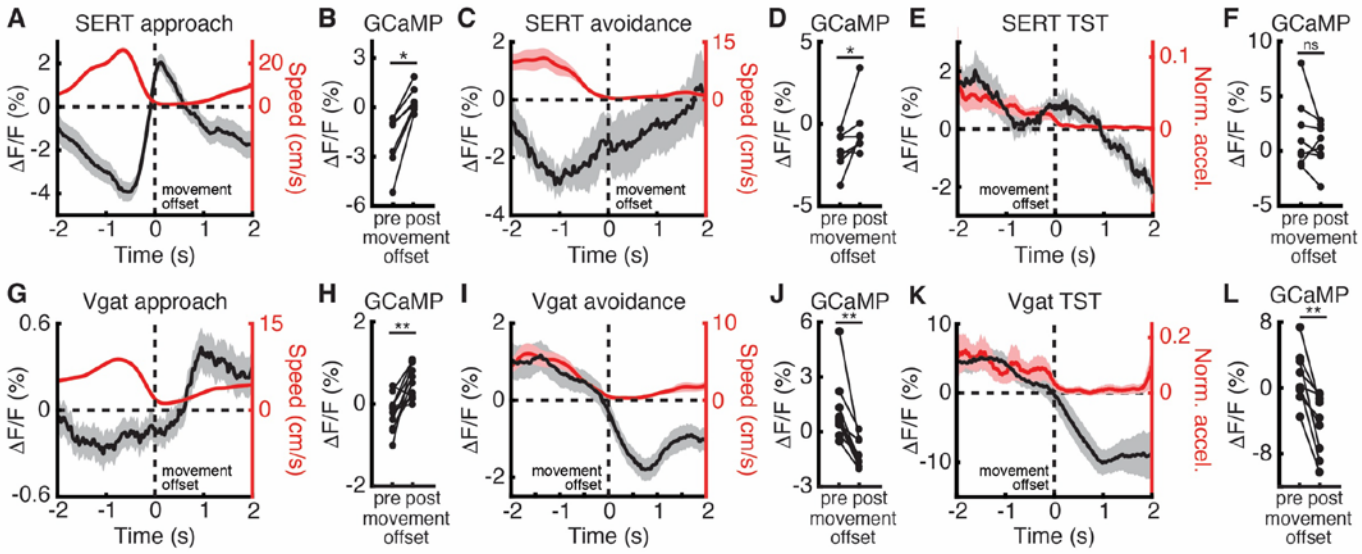

Fig. S3

(**A**) Mean ΔF/F aligned to approach movement offset from a SERT::GCaMP6s mouse. (**B**) Mean ΔF/F before (pre) and after (post) approach movement offset in SERT::GCaMP6s mice (n=7). (**C**) Mean ΔF/F aligned to avoidance movement offset from the mouse in panel A. (**D**) Mean ΔF/F before and after avoidance movement offset (n=7). (**E**) Mean ΔF/F aligned to TST movement offset from the mouse in panel A. (**F**) Mean ΔF/F before and after TST movement offset (n=8). (**G**) Mean ΔF/F aligned to approach movement offset from a Vgat::GCaMP6s mouse. (**H**) Mean ΔF/F before and after approach movement offset in Vgat::GCaMP6s mice (n=11). (**I**) Mean ΔF/F aligned to avoidance movement offset from the mouse in panel G. (**J**) Mean ΔF/F before and after avoidance movement offset (n=10). (**K**) Mean ΔF/F aligned to TST movement offset from the mouse in panel G. (**L**) Mean ΔF/F before and after TST movement offset (n=9) mice. **P* < 0.05, ***P* < 0.01 Wilcoxon signed-rank test. Error bars indicate s.e.m.

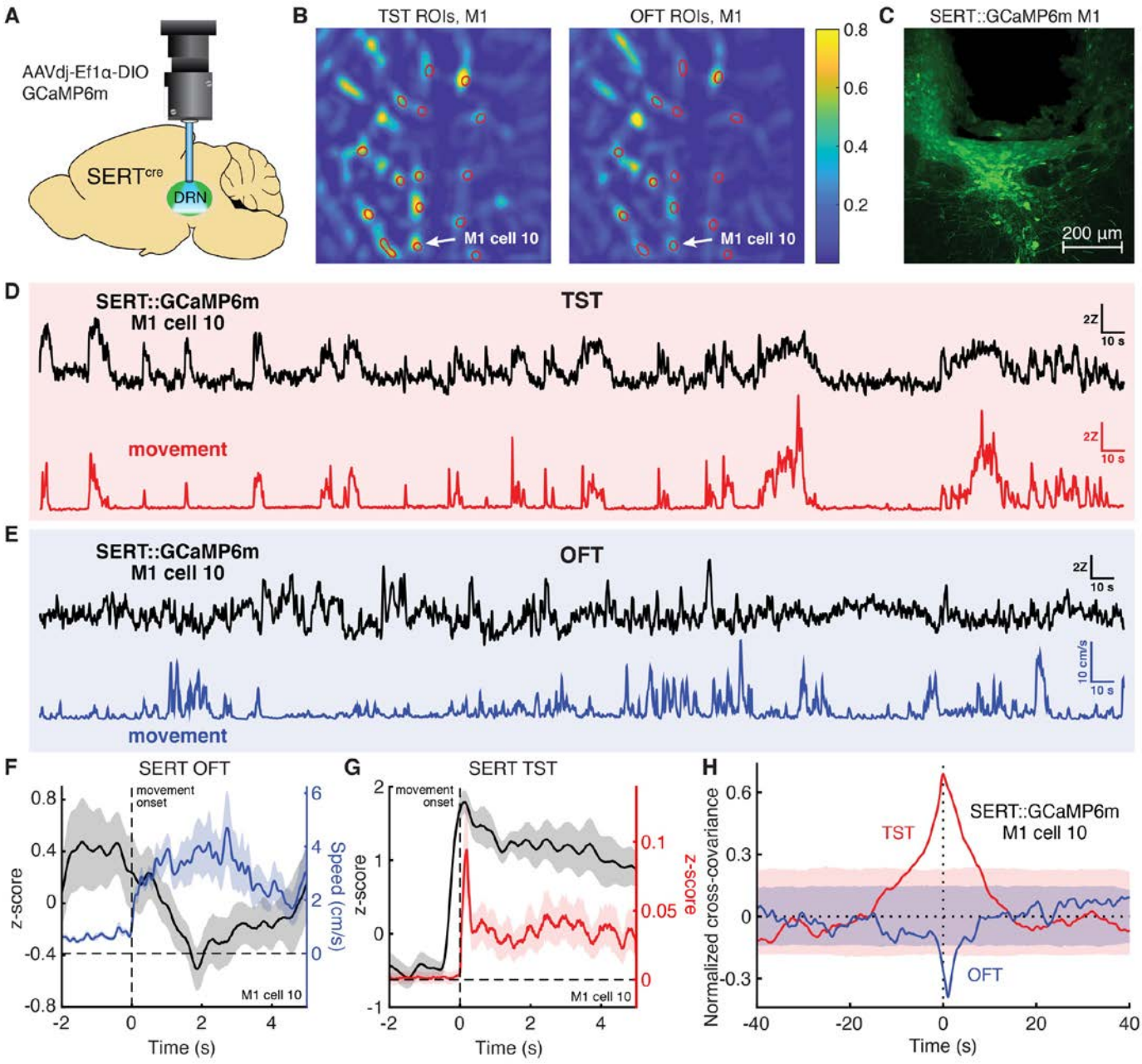

Fig. S4

(A) DRN microendoscopy schematic. (B) MIN1PIPE ROIs, TST and OFT. (C) GCaMP6m expression in mouse M1 DRN 5-HT neurons with GRIN lens track. (D) Example TST microendoscopy data from a mouse M1 DRN 5-HT single neuron. GCaMP activity in black, movement in red. (E) OFT data from the same neuron. GCaMP activity in black, movement in blue. (F) GCaMP6m activity aligned to TST movement onset for the same neuron. (G) GCaMP6m activity aligned to OFT movement onset for the same neuron. (H) Normalized cross-covariance between GCaMP6m activity and movement for the same

neuron in TST (red) and OFT (blue). Light red and blue regions indicate 99% bootstrap confidence intervals. Error bars indicate s.e.m.

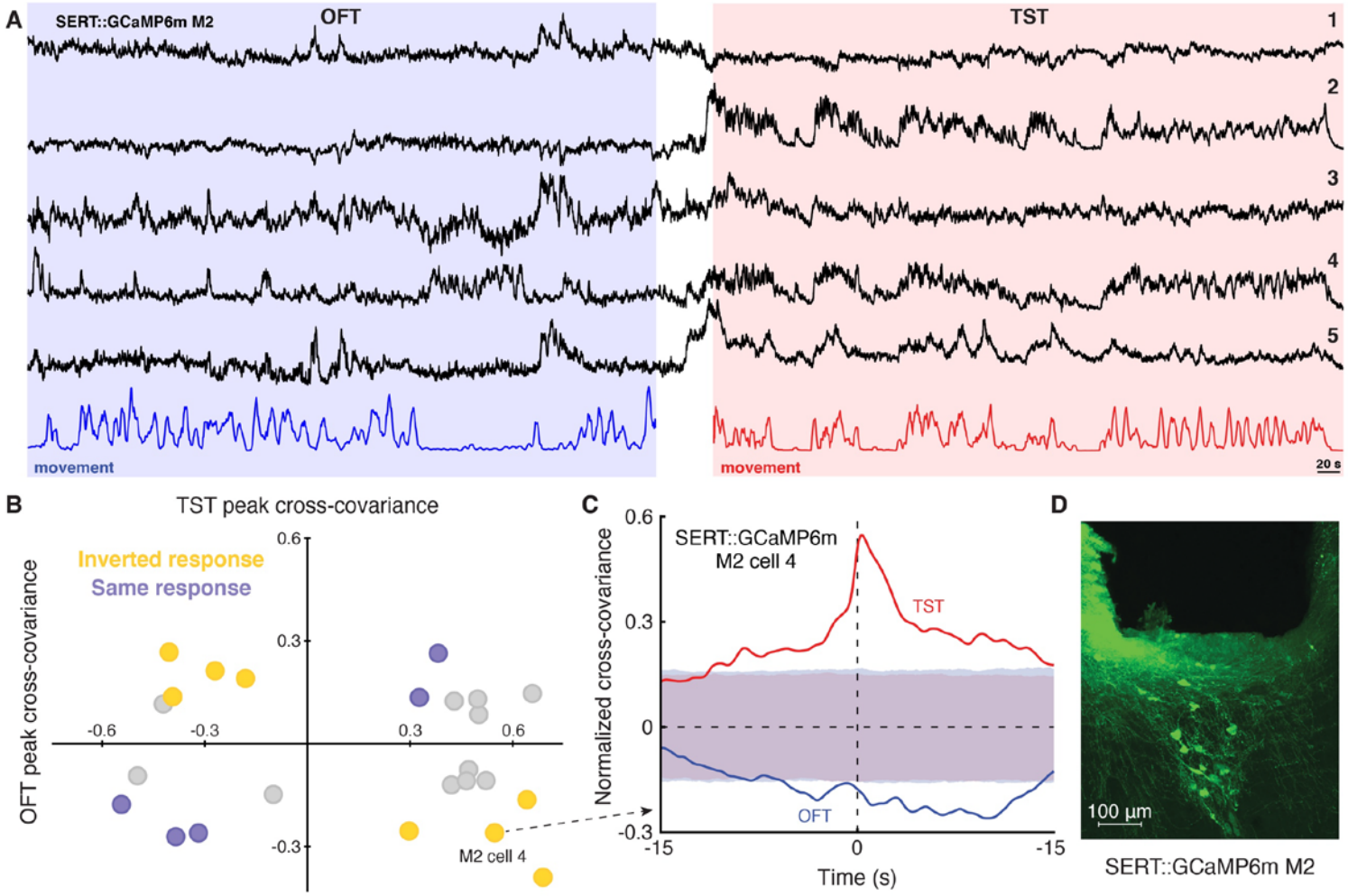

Fig. S5

(**A**) GCaMP6m activity from five DRN 5-HT neurons, continuously recorded during OFT and TST in mouse M2. GCaMP6m activity in black, OFT movement in blue, TST movement in red. (**B**) Peak normalized cross-covariance between movement and neural activity for all recorded DRN 5-HT neurons in OFT and TST environments. Cells with an inverted activity-movement relationship across environments in yellow, cells with the same activity-movement relationship in both environments in purple, cells without a significant movement response in one or both environments in gray. (**C**) Normalized cross-covariance between GCaMP6m activity and movement in TST (red) and OFT (blue) for a mouse M2 neuron. Light red and blue regions indicate 99% bootstrap confidence intervals. (**D**) GCaMP6m expression in mouse M2 DRN 5-HT neurons with GRIN lens track.

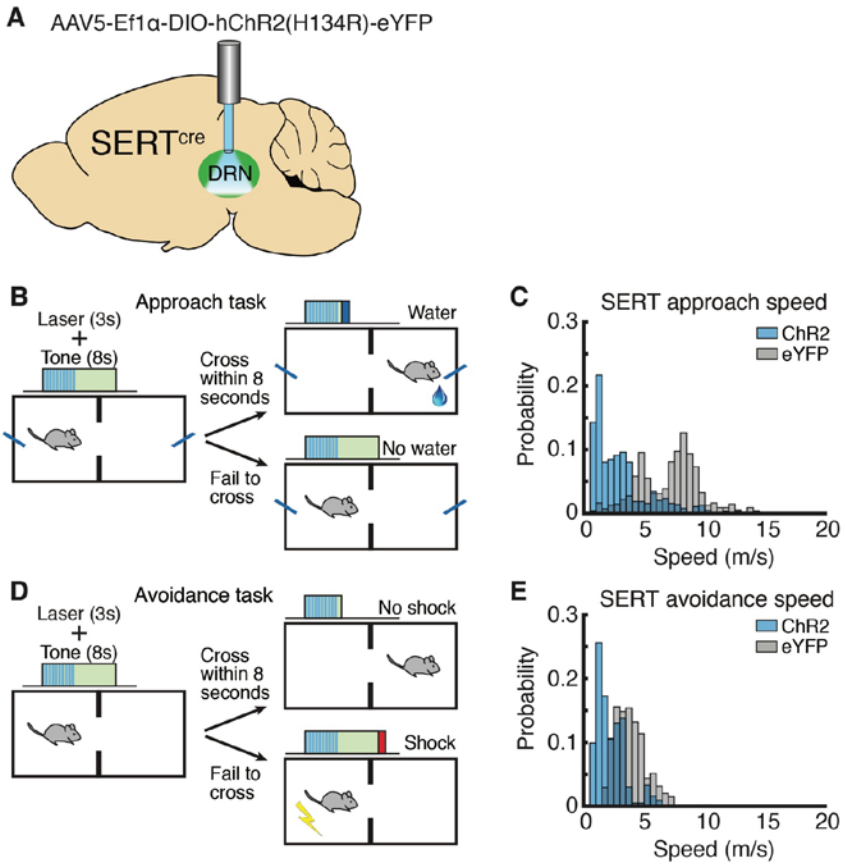

Fig. S6

(**A**) Dorsal raphe nucleus (DRN) ChR2-eYFP vector and optical fiber placement schematic. (**B**) Optogenetic stimulation schematic for approach task. (**C**) Speed distribution during stimulation in approach task (SERT::ChR2-eYFP, n=7; SERT::eYFP, n=6). (**D**) Optogenetic stimulation schematic for avoidance task. (**E**) Speed distribution during stimulation in avoidance task (SERT::ChR2-eYFP, n=7; SERT::eYFP, n=6).

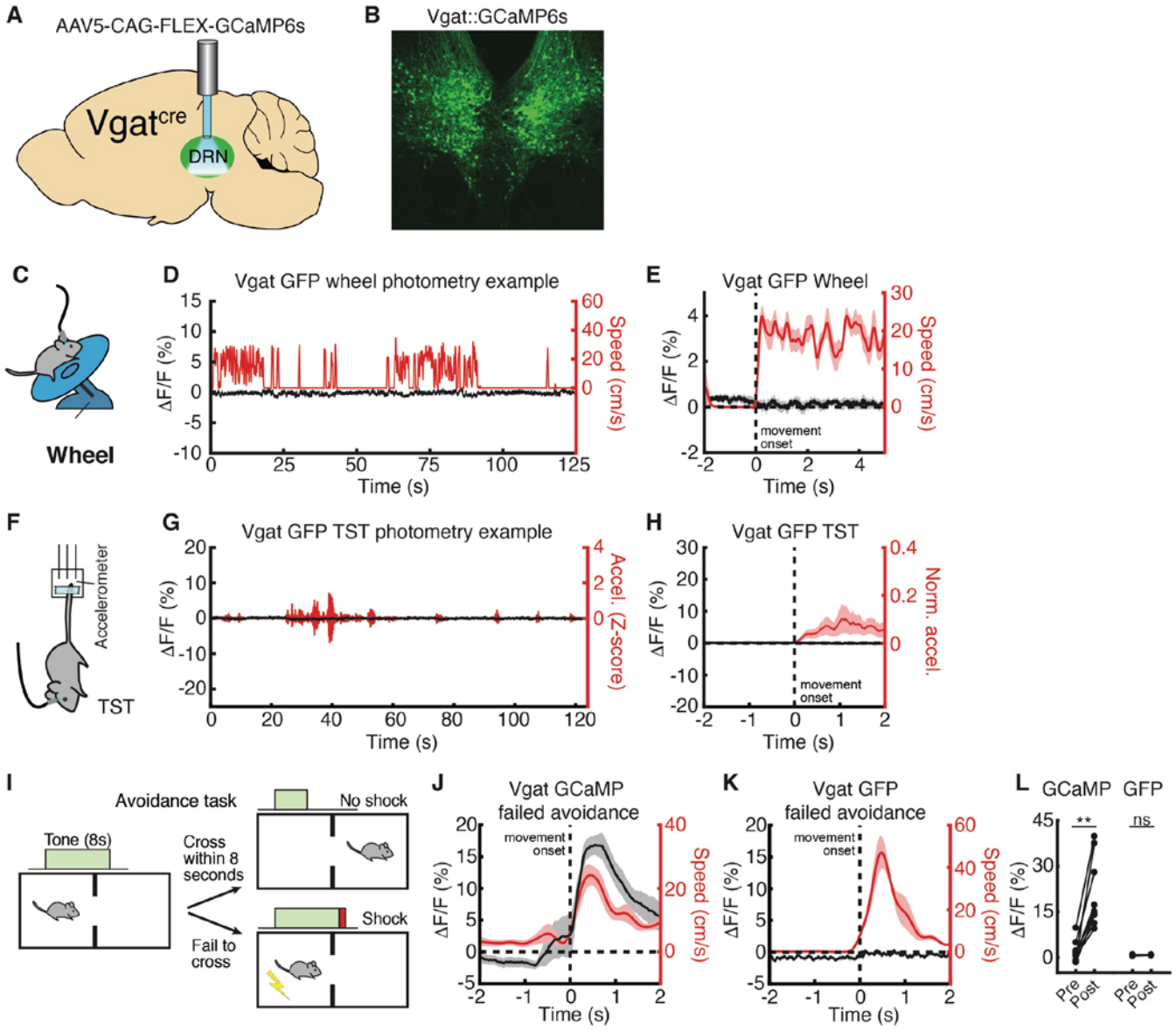

Fig. S7

(**A**) Dorsal raphe nucleus (DRN) viral vector and optical fiber placement schematic. (**B**) GCaMP6s expression in DRN GABA neurons in a Vgat-Cre mouse. (**C**) Wheel schematic. (**D**) Example wheel photometry data from a Vgat::GFP mouse. GFP ΔF/F in black, speed in red. (**E**) Mean ΔF/F aligned to wheel movement onset from the same mouse. (**F**) Tail suspension test (TST) schematic. (**G**) Example TST photometry data from a Vgat::GFP mouse. (**H**) Mean ΔF/F aligned to TST movement onset from the same mouse. (**I**) Avoidance task schematic. (**J**) Mean ΔF/F aligned to escape movement onset during failed avoidance trials from a Vgat::GCaMP6s mouse. (**K**) Mean ΔF/F aligned to escape movement onset during failed avoidance trials from a Vgat::GFP mouse. (**L**) Mean ΔF/F before and after movement onset to

escape the shock in GCaMP (n=10) and GFP (n=3) mice. **$P < 0.01$, Wilcoxon signed-rank test. Error bars indicate s.e.m.

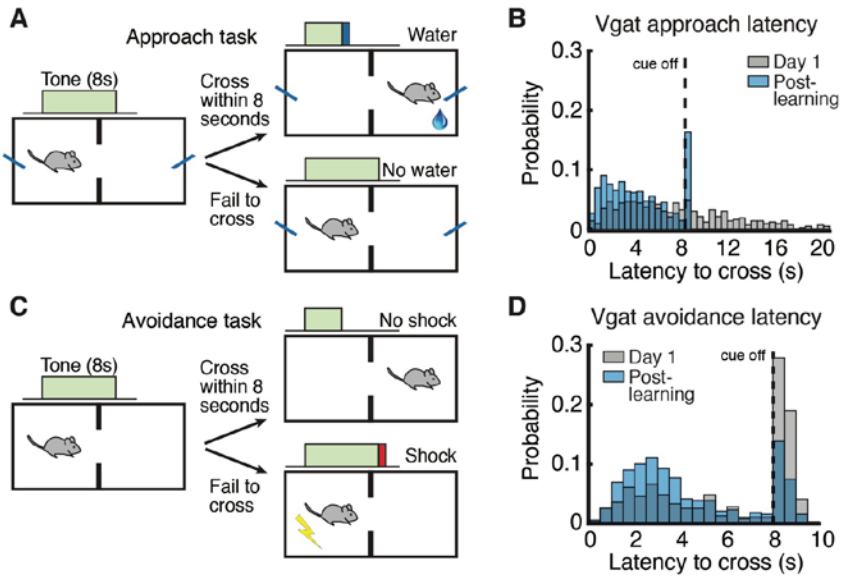

Fig. S8

(**A**) Approach task schematic. (**B**) Latency to cross after cue onset distribution, approach task, day 1 and post-learning (Vgat::GCaMP, n=11; $P < 0.0001$, log-rank test). Latency data were not collected for failed approach trials post-learning, but are binned here at 8 s for display only (not for statistical analysis). (**C**) Avoidance task schematic. (**D**) Latency to cross after cue onset distribution, avoidance task, day 1 and post-learning (Vgat::GCaMP, n=10; $P < 0.0001$, log-rank test).

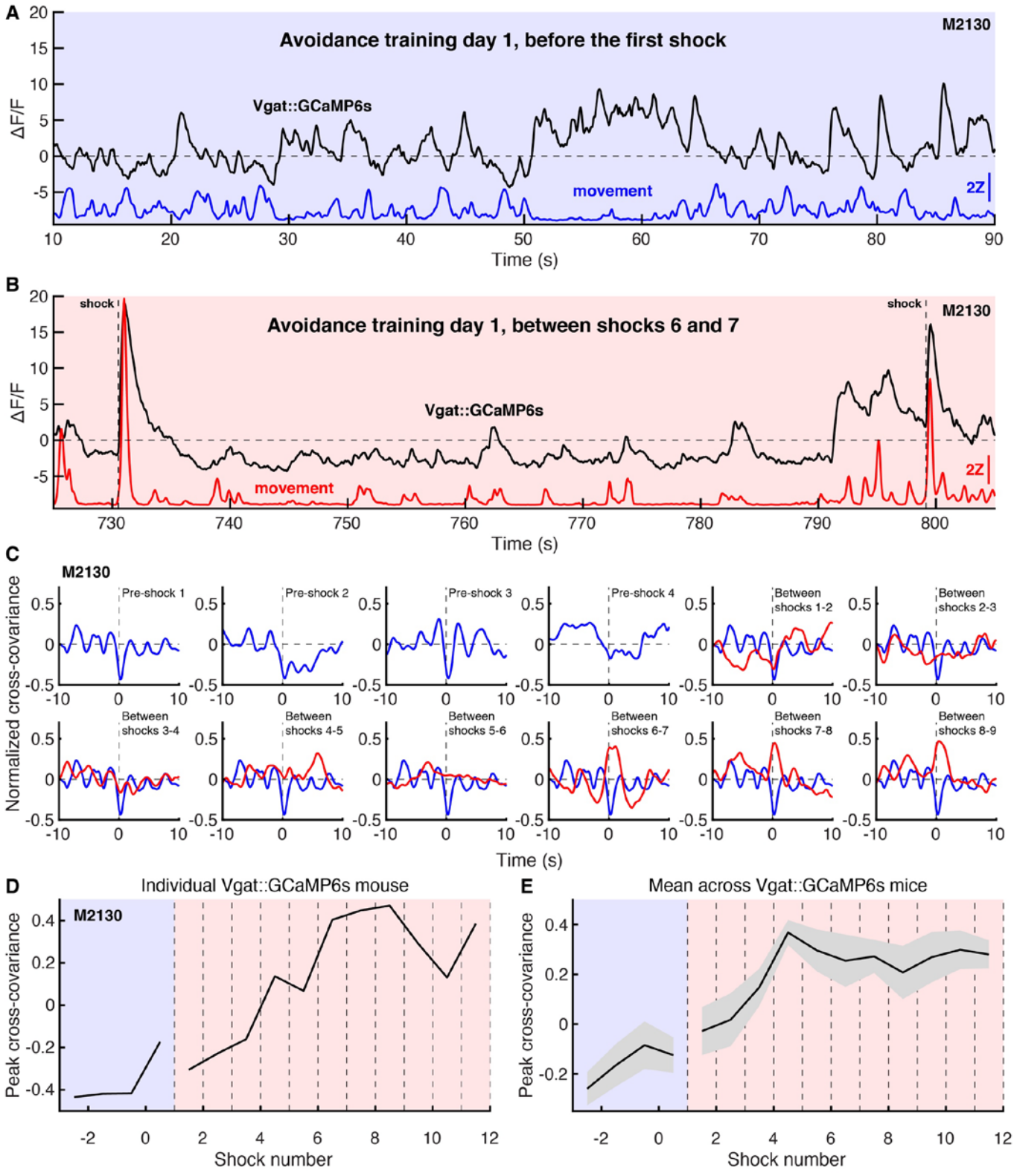
A
Avoidance training day 1, before the first shock
M2130
Vgat::GCaMP6s
movement
2Z
ΔF/F
Time (s)
B
Avoidance training day 1, between shocks 6 and 7
shock
shock
M2130
Vgat::GCaMP6s
movement
2Z
ΔF/F
Time (s)
C
M2130
Pre-shock 1
Pre-shock 2
Pre-shock 3
Pre-shock 4
Between shocks 1-2
Between shocks 2-3
Between shocks 3-4
Between shocks 4-5
Between shocks 5-6
Between shocks 6-7
Between shocks 7-8
Between shocks 8-9
Normalized cross-covariance
Time (s)
D
Individual Vgat::GCaMP6s mouse
M2130
Peak cross-covariance
Shock number
E
Mean across Vgat::GCaMP6s mice
Peak cross-covariance
Shock number

Fig. S9

(**A**) Example pre-shock photometry data from a Vgat::GCaMP6s mouse. GCaMP6s ΔF/F in black, speed in blue. (**B**) Example photometry data from the mouse in panel A following 6 shocks. GCaMP6s ΔF/F in black, speed in red. (**C**) Normalized cross-covariance between movement and GCaMP6s ΔF/F from the mouse in panel A during successive epochs of time. Pre-shock cross-covariance in blue, post-shock cross-covariance in red. Panels 5-12 include pre-shock panel 1 cross-covariance for comparison. (**D**) Peak cross-covariance during successive epochs from the same mouse. (**E**) Mean peak cross-covariance during successive epochs across mice. Error bars indicate s.e.m.

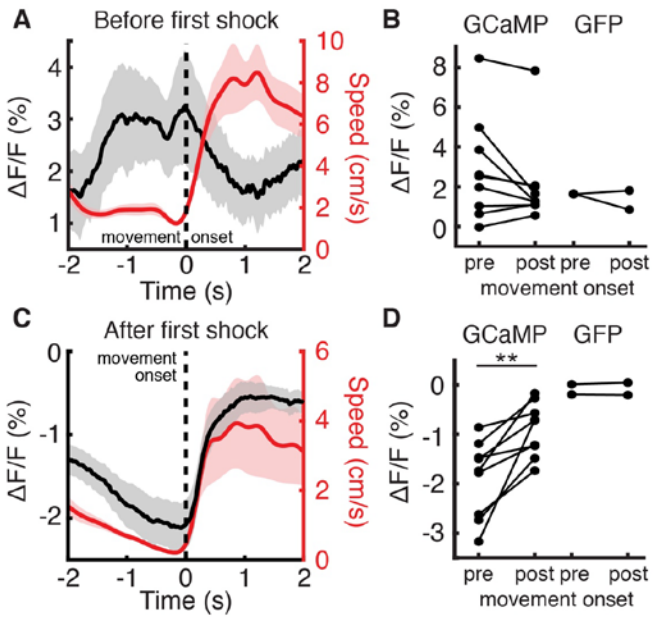

Fig. S10

(**A**) Mean DRN ΔF/F from a Vgat::GCaMP6s mouse aligned to movement onset, day 1 of avoidance training, before first shock. GCaMP ΔF/F in black, speed in red. (**B**) Mean ΔF/F before (pre) and after (post) movement onset in GCaMP (n=9) and GFP (n=2) mice, day 1 of avoidance training before first shock. (**C**) Mean ΔF/F aligned to movement onset from the mouse in panel A, same day after the first shock. (**D**) Mean ΔF/F before and after movement onset after the first shock in GCaMP (n=9) and GFP (n=2) mice. $^{**}P < 0.01$, Wilcoxon signed-rank test. Error bars indicate s.e.m.

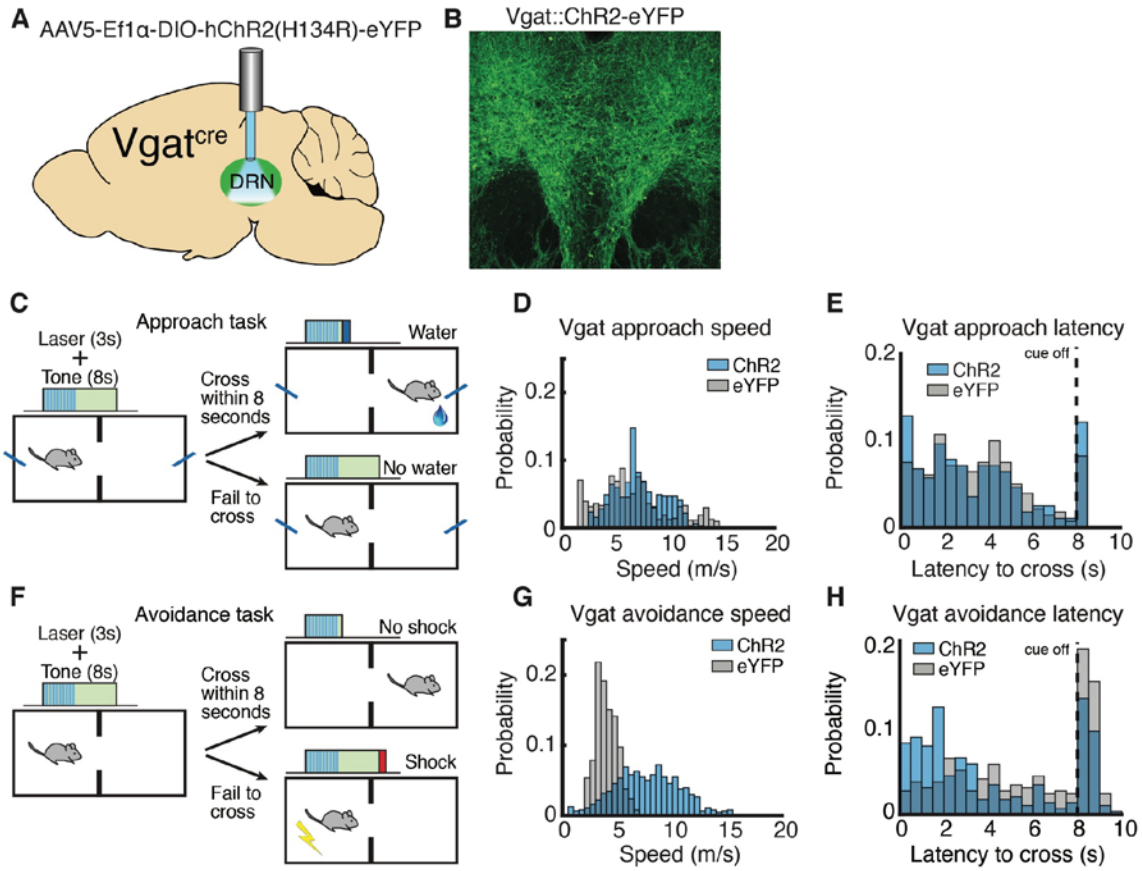

Fig. S11

(**A**) Dorsal raphe nucleus (DRN) viral vector and optical fiber placement schematic. (**B**) ChR2-eYFP expression in DRN GABA neurons in a Vgat-Cre mouse. (**C**) Optogenetic stimulation schematic in approach task. (**D**) Speed distribution during stimulation in approach task (Vgat::ChR2-eYFP, n=8; Vgat::eYFP, n=7). (**E**) Latency to cross after cue onset distribution, approach task. (Vgat::ChR2-eYFP, n=8; Vgat::eYFP, n=7; $P = 0.62$, log-rank test) (**F**) Optogenetic stimulation schematic in avoidance task. (**G**) Speed distribution during stimulation in avoidance task (Vgat::ChR2-eYFP, n=8; Vgat::eYFP, n=7). (**H**) Latency to cross after cue onset distribution, avoidance task (Vgat::ChR2-eYFP, n=8; Vgat::eYFP, n=7; $P < 0.0001$, log-rank test).

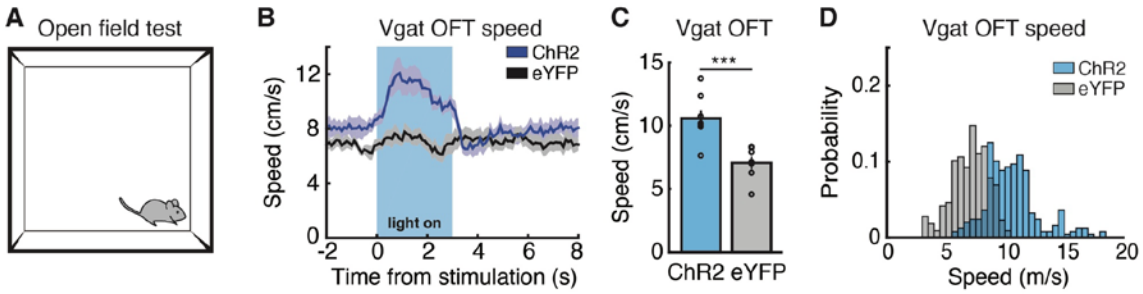

Fig. S12

(**A**) Open field test (OFT) schematic. (**B**) Speed aligned to stimulation onset, OFT (Vgat::ChR2-eYFP, n=8; Vgat::eYFP, n=7). (**C**) Mean speed during stimulation, OFT. (**D**) Speed distribution during stimulation in OFT. ***$P < 0.001$, Wilcoxon rank-sum test. Error bars indicate s.e.m.

Table S1.

Figure	Number of animals or trials	Statistical test	Comparison	Other information	Significance	*P*-value
1e (left)	n = 9	Wilcoxon sign-rank (two-sided)	Mean ΔF/F Pre (1.5s) vs Post (1.5s) movement onset		**	0.00391
1e (right)	n = 3	Wilcoxon sign-rank (two-sided)	Mean ΔF/F Pre (1.5s) vs Post (1.5s) movement onset		ns	1
1i	n = 7	Wilcoxon sign-rank (two-sided)	Mean ΔF/F Pre (1.5s) vs Post (1.5s) movement onset		*	0.03125
1m	n = 7	Wilcoxon sign-rank (two-sided)	Mean ΔF/F Pre (1.5s) vs Post (1.5s) movement onset		*	0.01563
2d (left)	n = 8	Wilcoxon sign-rank (two-sided)	Mean ΔF/F Pre (1.5s) vs Post (1.5s) movement onset		**	0.00781
2d (right)	n = 2	Wilcoxon sign-rank (two-sided)	Mean ΔF/F Pre (1.5s) vs Post (1.5s) movement onset		ns	0.5
2f	n = 7	Wilcoxon sign-rank (two-sided)	Mean ΔF/F Pre (1.5s) vs Post (1.5s) movement onset		*	0.01563
3c	ChR2 (n = 7) vs eYFP (n = 7)	Wilcoxon rank-sum (two-sided)	Mean speed during optogenetic stimulation (3s)		*	0.01107
3e	ChR2 (n = 7) vs eYFP (n = 6)	Wilcoxon rank-sum (two-sided)	Mean speed during optogenetic stimulation (3s)		**	0.00466
3f	ChR2 (n = 280) vs eYFP (n = 240)	Log-rank (Mantel-Cox) test (two-sided)	Comparison of survival curves	df = 1 χ^2 = 38.35	***	*P*<0.0001
3h	ChR2 (n = 7) vs eYFP (n = 6)	Wilcoxon rank-sum (two-sided)	Mean speed during optogenetic stimulation (3s)		*	0.02215
3i	ChR2 (n = 280) vs eYFP (n = 240)	Log-rank (Mantel-Cox) test (two-sided)	Comparison of survival curves	df = 1 χ^2 = 16.19	***	*P*<0.0001
3k	ChR2 (n = 7) vs eYFP (n = 6)	Wilcoxon rank-sum (two-sided)	Difference in mean acceleration between Pre (-2s to 0s) and Post (0s to 3s) optogenetic stimulation (3s) onset		*	0.03496
4c	n = 10	Wilcoxon sign-rank (two-sided)	Mean ΔF/F Pre (1.5s) vs Post (1.5s) movement onset		**	0.00977
4e	ChR2 (n = 8) vs eYFP (n = 7)	Wilcoxon rank-sum (two-sided)	Mean speed during optogenetic stimulation (3s)		ns	0.62279
4h	n = 10	Wilcoxon sign-rank (two-sided)	Mean ΔF/F Pre (1.5s) vs Post (1.5s) movement onset		**	0.00195
4j	ChR2 (n = 8) vs eYFP (n = 7)	Wilcoxon rank-sum (two-sided)	Mean speed during optogenetic stimulation (3s)		***	0.00037
4n (left)	n = 9	Wilcoxon sign-rank (two-sided)	Mean ΔF/F Pre (1.5s) vs Post (1.5s) movement onset		**	0.00391
4n (right)	n = 3	Wilcoxon sign-rank (two-sided)	Mean ΔF/F Pre (1.5s) vs Post (1.5s) movement onset		ns	0.5
4o	ChR2 (n = 7) vs eYFP (n = 7)	Wilcoxon rank-sum (two-sided)	Mean time spent running during stimulation		ns	0.9015
4s (left)	n = 9	Wilcoxon sign-rank (two-sided)	Mean ΔF/F Pre (1.5s) vs Post (1.5s) movement onset		**	0.00391
4s (right)	n = 3	Wilcoxon sign-rank (two-sided)	Mean ΔF/F Pre (1.5s) vs Post (1.5s) movement onset		ns	0.75
4t	ChR2 (n = 7) vs eYFP (n = 7)	Wilcoxon rank-sum (two-sided)	Mean time spent struggling during stimulation		**	0.007
2Sb	Day 1 (n = 210) vs Post-learning (n = 210)	Log-rank (Mantel-Cox) test (two-sided)	Comparison of survival curves	df = 1 χ^2 = 81.81	***	*P*<0.0001
2Sd	Day 1 (n = 210) vs Post-learning (n = 280)	Log-rank (Mantel-Cox) test (two-sided)	Comparison of survival curves	df = 1 χ^2 = 54.57	***	*P*<0.0001
4Sl (left)	n = 10	Wilcoxon sign-rank (two-sided)	Mean ΔF/F Pre (1.5s) vs Post (1.5s) movement onset		**	0.00195
4Sl (right)	n = 3	Wilcoxon sign-rank (two-sided)	Mean ΔF/F Pre (1.5s) vs Post (1.5s) movement onset		ns	1
5Sb	Day 1 (n = 434) vs Post-learning (n = 489)	Log-rank (Mantel-Cox) test (two-sided)	Comparison of survival curves	df = 1 χ^2 = 105.2	***	*P*<0.0001
5Sd	Day 1 (n = 395) vs Post-learning (n = 389)	Log-rank (Mantel-Cox) test (two-sided)	Comparison of survival curves	df = 1 χ^2 = 70.91	***	*P*<0.0001
6Sd	ChR2 (n = 280) vs eYFP (n = 280)	Log-rank (Mantel-Cox) test (two-sided)	Comparison of survival curves	df = 1 χ^2 = 0.2457	ns	0.6201
6Sg	ChR2 (n = 280) vs eYFP (n = 280)	Log-rank (Mantel-Cox) test (two-sided)	Comparison of survival curves	df = 1 χ^2 = 24.17	***	*P*<0.0001
7Sc	ChR2 (n = 8) vs eYFP (n = 7)	Wilcoxon rank-sum (two-sided)	Mean speed during optogenetic stimulation (3s)		***	0.00097

References

1. M. S. Fanselow, Neural organization of the defensive behavior system responsible for fear. *Psychon. Bull. Rev.* **1**, 429–438 (1994). doi:10.3758/BF03210947 Medline

2. G. De Franceschi, T. Vivattanasarn, A. B. Saleem, S. G. Solomon, Vision Guides Selection of Freeze or Flight Defense Strategies in Mice. *Curr. Biol.* **26**, 2150–2154 (2016). doi:10.1016/j.cub.2016.06.006 Medline

3. R. C. Ydenberg, L. M. Dill, The economics of fleeing from predators. *Adv. Stud. Behav.* **16**, 229–249 (1986). doi:10.1016/S0065-3454(08)60192-8

4. S. K. Ogawa, J. Y. Cohen, D. Hwang, N. Uchida, M. Watabe-Uchida, Organization of monosynaptic inputs to the serotonin and dopamine neuromodulatory systems. *Cell Rep.* **8**, 1105–1118 (2014). doi:10.1016/j.celrep.2014.06.042 Medline

5. Y. Niv, N. D. Daw, D. Joel, P. Dayan, Tonic dopamine: Opportunity costs and the control of response vigor. *Psychopharmacology* **191**, 507–520 (2007). doi:10.1007/s00213-006-0502-4 Medline

6. J. D. Salamone, M. Pardo, S. E. Yohn, L. López-Cruz, N. SanMiguel, M. Correa, Mesolimbic dopamine and the regulation of motivated behavior. *Curr. Top. Behav. Neurosci.* **27**, 231–257 (2016). doi:10.1007/7854_2015_383 Medline

7. P. Soubrié, Reconciling the role of central serotonin neurons in human and animal behavior. *Behav. Brain Sci.* **9**, 319 (1986). doi:10.1017/S0140525X00022871

8. J. F. W. Deakin, F. G. Graeff, 5-HT and mechanisms of defence. *J. Psychopharmacol.* **5**, 305–315 (1991). doi:10.1177/026988119100500414 Medline

9. K. W. Miyazaki, K. Miyazaki, K. F. Tanaka, A. Yamanaka, A. Takahashi, S. Tabuchi, K. Doya, Optogenetic activation of dorsal raphe serotonin neurons enhances patience for future rewards. *Curr. Biol.* **24**, 2033–2040 (2014). doi:10.1016/j.cub.2014.07.041 Medline

10. P. A. Correia, E. Lottem, D. Banerjee, A. S. Machado, M. R. Carey, Z. F. Mainen, Transient inhibition and long-term facilitation of locomotion by phasic optogenetic activation of serotonin neurons. *eLife* **6**, e20975 (2017). doi:10.7554/eLife.20975 Medline

11. C. A. Marcinkiewcz, C. M. Mazzone, G. D'Agostino, L. R. Halladay, J. A. Hardaway, J. F. DiBerto, M. Navarro, N. Burnham, C. Cristiano, C. E. Dorrier, G. J. Tipton, C. Ramakrishnan, T. Kozicz, K. Deisseroth, T. E. Thiele, Z. A. McElligott, A. Holmes, L. K. Heisler, T. L. Kash, Serotonin engages an anxiety and fear-promoting circuit in the extended amygdala. *Nature* **537**, 97–101 (2016). doi:10.1038/nature19318 Medline

12. A. A. Harrison, B. J. Everitt, T. W. Robbins, Central 5-HT depletion enhances impulsive responding without affecting the accuracy of attentional performance: Interactions with

dopaminergic mechanisms. *Psychopharmacology* **133**, 329–342 (1997). doi:10.1007/s002130050410 Medline

13. H. F. Clarke, J. W. Dalley, H. S. Crofts, T. W. Robbins, A. C. Roberts, Cognitive inflexibility after prefrontal serotonin depletion. *Science* **304**, 878–880 (2004). doi:10.1126/science.1094987 Medline

14. J. F. Cryan, A. Markou, I. Lucki, Assessing antidepressant activity in rodents: Recent developments and future needs. *Trends Pharmacol. Sci.* **23**, 238–245 (2002). doi:10.1016/S0165-6147(02)02017-5 Medline

15. M. R. Warden, A. Selimbeyoglu, J. J. Mirzabekov, M. Lo, K. R. Thompson, S.-Y. Kim, A. Adhikari, K. M. Tye, L. M. Frank, K. Deisseroth, A prefrontal cortex-brainstem neuronal projection that controls response to behavioural challenge. *Nature* **492**, 428–432 (2012). doi:10.1038/nature11617 Medline

16. L. A. Gunaydin, L. Grosenick, J. C. Finkelstein, I. V. Kauvar, L. E. Fenno, A. Adhikari, S. Lammel, J. J. Mirzabekov, R. D. Airan, K. A. Zalocusky, K. M. Tye, P. Anikeeva, R. C. Malenka, K. Deisseroth, Natural neural projection dynamics underlying social behavior. *Cell* **157**, 1535–1551 (2014). doi:10.1016/j.cell.2014.05.017 Medline

17. T.-W. Chen, T. J. Wardill, Y. Sun, S. R. Pulver, S. L. Renninger, A. Baohan, E. R. Schreiter, R. A. Kerr, M. B. Orger, V. Jayaraman, L. L. Looger, K. Svoboda, D. S. Kim, Ultrasensitive fluorescent proteins for imaging neuronal activity. *Nature* **499**, 295–300 (2013). doi:10.1038/nature12354 Medline

18. X. Zhuang, J. Masson, J. A. Gingrich, S. Rayport, R. Hen, Targeted gene expression in dopamine and serotonin neurons of the mouse brain. *J. Neurosci. Methods* **143**, 27–32 (2005). doi:10.1016/j.jneumeth.2004.09.020 Medline

19. K. G. Commons, A. B. Cholanians, J. A. Babb, D. G. Ehlinger, The rodent forced swim test measures stress-coping strategy, not depression-like behavior. *ACS Chem. Neurosci.* **8**, 955–960 (2017). doi:10.1021/acschemneuro.7b00042 Medline

20. Y. Ziv, L. D. Burns, E. D. Cocker, E. O. Hamel, K. K. Ghosh, L. J. Kitch, A. El Gamal, M. J. Schnitzer, Long-term dynamics of CA1 hippocampal place codes. *Nat. Neurosci.* **16**, 264–266 (2013). doi:10.1038/nn.3329 Medline

21. E. S. Boyden, F. Zhang, E. Bamberg, G. Nagel, K. Deisseroth, Millisecond-timescale, genetically targeted optical control of neural activity. *Nat. Neurosci.* **8**, 1263–1268 (2005). doi:10.1038/nn1525 Medline

22. L. Vong, C. Ye, Z. Yang, B. Choi, S. Chua Jr., B. B. Lowell, Leptin action on GABAergic neurons prevents obesity and reduces inhibitory tone to POMC neurons. *Neuron* **71**, 142–154 (2011). doi:10.1016/j.neuron.2011.05.028 Medline

23. L. Bonanni, A. Thomas, M. Onofrj, Paradoxical kinesia in parkinsonian patients surviving earthquake. *Mov. Disord.* **25**, 1302–1304 (2010). doi:10.1002/mds.23075 Medline

24. J. F. Marshall, D. Levitan, E. M. Stricker, Activation-induced restoration of sensorimotor functions in rats with dopamine-depleting brain lesions. *J. Comp. Physiol. Psychol.* **90**, 536–546 (1976). doi:10.1037/h0077230 Medline

25. O. F. O'Leary, A. J. Bechtholt, J. J. Crowley, R. J. Valentino, I. Lucki, The role of noradrenergic tone in the dorsal raphe nucleus of the mouse in the acute behavioral effects of antidepressant drugs. *Eur. Neuropsychopharmacol.* **17**, 215–226 (2007). doi:10.1016/j.euroneuro.2006.06.012 Medline

26. M. Waselus, C. Nazzaro, R. J. Valentino, E. J. Van Bockstaele, Stress-induced redistribution of corticotropin-releasing factor receptor subtypes in the dorsal raphe nucleus. *Biol. Psychiatry* **66**, 76–83 (2009). doi:10.1016/j.biopsych.2009.02.014 Medline

27. S. Puglisi-Allegra, D. Andolina, Serotonin and stress coping. *Behav. Brain Res.* **277**, 58–67 (2015). doi:10.1016/j.bbr.2014.07.052 Medline

28. J. Amat, M. V. Baratta, E. Paul, S. T. Bland, L. R. Watkins, S. F. Maier, Medial prefrontal cortex determines how stressor controllability affects behavior and dorsal raphe nucleus. *Nat. Neurosci.* **8**, 365–371 (2005). doi:10.1038/nn1399 Medline

29. J. Lu, C. Li, J. Singh-Alvarado, Z. C. Zhou, F. Fröhlich, R. Mooney, F. Wang, MIN1PIPE: A Miniscope 1-Photon-Based Calcium Imaging Signal Extraction Pipeline. *Cell Rep.* **23**, 3673–3684 (2018). doi:10.1016/j.celrep.2018.05.062 Medline

30. D. N. Politis, J. P. Romano, The Stationary Bootstrap. *J. Am. Stat. Assoc.* **89**, 1303–1313 (1994). doi:10.1080/01621459.1994.10476870